Observations of Co^{4+} in a Higher Spin State and the Increase in the Seebeck Coefficient of Thermoelectric $Ca_3Co_4O_9$

R. F. Klie, Q. Qiao, T. Paulauskas, A. Gulec, A. Rebola, and S. Öğüt
Department of Physics, University of Illinois at Chicago, Chicago, Illinois, USA

M. P. Prange,[1,2] J. C. Idrobo,[2] and S. T. Pantelides[1,2]
[1]*Department of Physics and Astronomy, Vanderbilt University, Nashville, Tennessee, USA*
[2]*Materials Science and Technology Division, Oak Ridge National Laboratory, Oak Ridge, Tennessee, USA*

S. Kolesnik and B. Dabrowski
Department of Physics, Northern Illinois University, DeKalb, Illinois, USA
and Materials Science Division, Argonne National Laboratory, Argonne, Illinois, USA

M. Ozdemir, C. Boyraz, D. Mazumdar, and A. Gupta
Center of Materials for Information Technology, University of Alabama, Tuscaloosa, Alabama, USA
and Department of Physics, Marmara University, Istanbul, Turkey
(Received 25 August 2011; published 8 May 2012)

$Ca_3Co_4O_9$ has a unique structure that leads to exceptionally high thermoelectric transport. Here we report the achievement of a 27% increase in the room-temperature in-plane Seebeck coefficient of $Ca_3Co_4O_9$ thin films. We combine aberration-corrected Z-contrast imaging, atomic-column resolved electron energy-loss spectroscopy, and density-functional calculations to show that the increase is caused by stacking faults with Co^{4+}-ions in a higher spin state compared to that of bulk $Ca_3Co_4O_9$. The higher Seebeck coefficient makes the $Ca_3Co_4O_9$ system suitable for many high temperature waste-heat-recovery applications.

DOI: 10.1103/PhysRevLett.108.196601 PACS numbers: 72.20.Pa, 68.37.Lp, 75.50.Pp, 79.20.Uv

Thermoelectric (TE) materials have attracted increasing attention over the last two decades, when theoretical predictions suggested that the TE efficiency could be enhanced through nanostructural engineering, which led to experimental studies demonstrating proof-of-principle high-efficiency materials [1]. Initially, complex bulk materials were found to exhibit high TE efficiencies [2–4], followed by nanostructured Bi_2Te_3-Bi_2Se_3 superlattices which showed a TE figure of merit (zT) in excess of 2 at room temperature [5].

The focus of research on TE devices has since shifted primarily to nanostructures, such as quantum dots, superlattices, or nanowires. However, many of these systems are unstable at high temperatures and toxic. They are also difficult and expensive to synthesize for large-scale applications. Layered complex oxides such as $Ca_3Co_4O_9$ exhibit large in-plane TE transport behavior, are stable at high temperatures, and contain mostly cheap and nontoxic elements.

$Ca_3Co_4O_9$ is an incommensurately layered oxide, consisting of two separate subsystems, CoO_2 and Ca_2CoO_3, each fulfilling a different role in achieving remarkably high TE properties at room and elevated temperature. Along the c-axis of $Ca_3Co_4O_9$, CdI_2-type CoO_2 layers are separated by a triple-layer of insulating rocksalt-type Ca_2CoO_3. The CoO_2 acts as the highly conductive hole-doped electron crystal. The insulating Ca_2CoO_3 acts as the phonon-glass and charge reservoir layers.

The high Seebeck coefficient in $Ca_3Co_4O_9$ has been attributed to a number of different mechanisms, including the occurrence of a mixed-valence state in the CoO_2 layer [6], or the increased entropy of the localized electrons in the degenerated cobalt $3d$ states [7]. Several studies have suggested that varying the compressive strain on the CoO_2 subsystem could provide a viable path to further increase the Seebeck coefficient, S, in $Ca_3Co_4O_9$ [8–10]. There appear to be two ways of exerting further compressive strain on the CoO_2 subsystem, by doping the rocksalt layers or by epitaxial thin-film growth on lattice mismatched substrates. While there is a large number of doping studies showing moderate increases in either the Seebeck coefficient or the electrical conductivity of bulk $Ca_3Co_4O_9$ (see, for example, Refs. [11,12]), detailed thin film studies [13] have shown that pristine $Ca_3Co_4O_9$ films grow largely unstrained on a variety of oxide substrates and do not exhibit any significant increase in the in-plane Seebeck coefficient. Furthermore, an in-depth survey of the published literature reveals that the Seebeck coefficient of pristine bulk $Ca_3Co_4O_9$ is limited to $S_{max} \approx 135\ \mu V/K$ at room temperature (see, for example, [14]), suggesting the presence of a fundamental limit to further increasing the thermoelectric properties of layered cobalt oxides.

In this Letter, we demonstrate that controlling the defect structure in $Ca_3Co_4O_9$ thin films can hold the key to further increasing the Seebeck coefficient. By synthesizing highly textured $Ca_3Co_4O_9$ films with a large concentration of CoO_2 stacking faults, we are able to increase the in-plane Seebeck coefficient from $S_{bulk} \approx 135\ \mu V/K$, in bulk, to $S_{film} \approx 180\ \mu V/K$ in thin $Ca_3Co_4O_9$ films at room temperature, while maintaining an electrical resistivity of $10.5 \pm 0.5\ m\Omega\,cm$ [see insert in Fig. 1(a)]. We attribute the large concentration of stacking faults to the rapid growth dynamics and the reduced thickness of the films. Using a combination of atomically-resolved Z-contrast imaging and electron energy-loss spectroscopy (EELS) in aberration-corrected scanning transmission electron microscopy (STEM), and first-principles calculations, we show that the high Seebeck coefficient in $Ca_3Co_4O_9$ thin films on $SrTiO_3$ [001] is due to the presence of CoO_2 stacking faults, which stabilize the transition of Co^{4+}-ions from a low spin-state in bulk $Ca_3Co_4O_9$ to an intermediate spin in the thin films at room temperature and above.

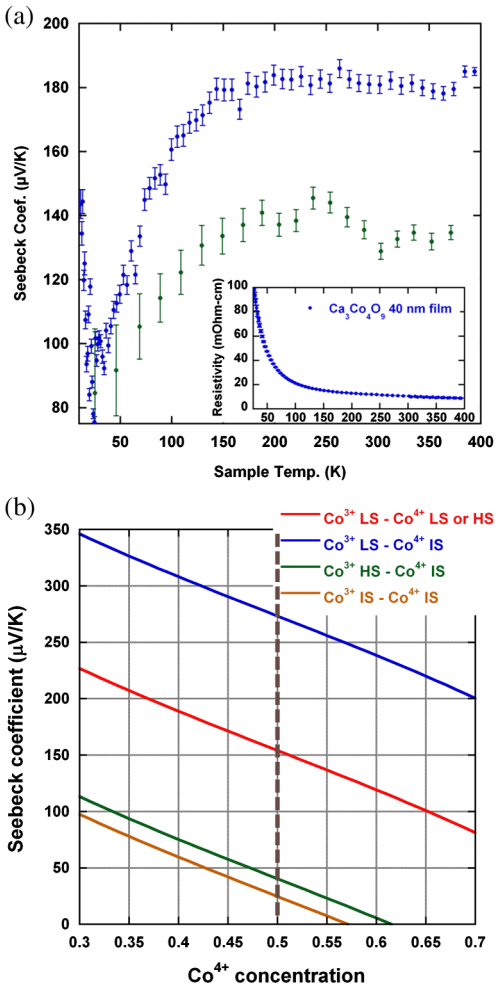

FIG. 1 (color online). (a) Seebeck coefficients for thin film and bulk $Ca_3Co_4O_9$. Insert: In-plane electrical resistivity as a function of temperature T. (b) Calculated Seebeck coefficients using Eq. (1) for different spin states as a function of cobalt valence in the CoO_2 layers. The dashed line shows the Co^{4+} concentration found in the CoO_2 layers.

Figure 1(a) shows the in-plane Seebeck coefficient in the temperature range between 10 K and 400 K of the nominally 40 nm thick $Ca_3Co_4O_9$ films on $SrTiO_3$ and of highly textured $Ca_3Co_4O_9$ bulk. For temperatures 25 K, we find a significant increase in the Seebeck coefficient with decreasing temperature as previously reported by Tang *et al.* [15] In the low temperature regime above 25 K, both samples show the typical linear dependence of the Seebeck coefficient with temperature, suggesting a Fermi-liquid behavior [16]. When plotting the Seebeck coefficient as a function of the normalized Fermi temperature, as suggested by Limette *et al.* [16], we find that the bulk and thin film $Ca_3Co_4O_9$ exhibit the same linear temperature dependence of the Seebeck coefficient (see Supplemental Materials Fig. S2 [17]).

At temperatures higher than 200 K, the in-plane Seebeck coefficient reaches a plateau. However, the value of the Seebeck coefficient in this regime is significantly higher in the $Ca_3Co_4O_9$ thin films compared to any reported bulk $Ca_3Co_4O_9$ values. The high-temperature behavior of the Seebeck coefficient in $Ca_3Co_4O_9$ is governed by the Heikes formula,

$$S = \frac{k_B}{e} \ln\left(\frac{g_{3+}}{g_{4+}} \frac{1-x}{x}\right), \tag{1}$$

where x is the Co^{4+} concentration, g_{3+} and g_{4+} are the orbital degeneracy of Co^{3+} and Co^{4+} in the CoO_2-layers. We have previously shown that the CoO_2-layers in bulk $Ca_3Co_4O_9$ are highly hole-doped, resulting in a mixed Co valence state with $x = 0.5$ [18].

Figure 1(b) shows the calculated Seebeck coefficient using Eq. (1) for different Co^{3+} and Co^{4+} spin states, including the Co^{3+} low spin state (LS, $t_{2g}^6 e_g^0$), the Co^{3+} intermediate-spin state (IS, $t_{2g}^5 e_g^1$), the Co^{3+} high-spin state (HS, $t_{2g}^4 e_g^2$), as well as the Co^{4+} low-spin state (LS, $t_{2g}^5 e_g^0$) and Co^{4+} intermediate-spin state (IS, $t_{2g}^4 e_g^1$). It is generally accepted that both the Co^{3+} and Co^{4+}-ions in the CoO_2-layers are in the low spin state for undoped bulk, thereby imposing an upper limit on the Seebeck coefficient for $x = 0.5$ of $S \approx 154\ \mu V/K$, as widely observed experimentally at room temperature. Our measured value of the in-plane Seebeck coefficient of $S_{bulk} = 135\ \mu V/K$ is therefore very close to this limit, yet the measured Seebeck coefficient in the thin film, $S_{film} = 180\ \mu V/K$, cannot be explained using this model, or any modified version, such as the one proposed by Pollet *et al.* [19]. We believe that the increase in the Seebeck coefficient will also be observed at temperatures higher than 400 K.

The increase in the Co^{4+}-ion spin state results in a larger contribution to the Seebeck coefficient as shown in Fig. 1, with a new upper limit of $S_{max} \approx 275\ \mu V/K$. The result suggests that stacking faults within the incommensurably layered $Ca_3Co_4O_9$ provide a significant fraction

of Co^{4+}-ions in the intermediate-spin state to the CoO_2-layers.

Figures 2(a) and 2(b) show atomic-resolution *Z*-contrast images of the $Ca_3Co_4O_9$ thin-film on $SrTiO_3$. Our imaging study shows that the average film thickness is 30 nm. Some regions of the image show $Ca_3Co_4O_9$ along the [110] direction, with the Ca_2CoO_3 layer exhibiting the usual trilayer structure [see Fig. 2(d)], while in other areas the structure appears to be rotated out of the zone-axis orientation. Such interlayer rotation along the *c*-direction has not been observed in any of the previously analyzed $Ca_3Co_4O_9$ thin films deposited on either $SrTiO_3$ $LaAlO_3$, or $(La_{0.3}Sr_{0.7})(Al_{0.65}Ta_{0.35})O_3$ [13]. In addition to this in-plane rotation, the images also show stacking faults in the form of double CoO_2 layers. The influence of stacking faults, which are found on average every 10 unit-cell in the thin film, and the effects of the interlayer rotation on the thermoelectric transport properties will be discussed next.

Two-dimensional atomically-resolved EEL spectrum images (SI) were acquired from the thin films, and the Co $L_{2,3}$-ratio was used to determine the doping concentration in the CoO_2-layers in bulk $Ca_3Co_4O_9$ [18,20]. Similar to bulk, we find that the Co valence in the CoO_2-layers of the thin films is 3.5 ± 0.1 [see insert in Fig. 2(c) and Supplemental Materials Fig. S3 [17]]. No change in the Co valence in the CoO_2 stacking faults or the CoO_2 layers between two rotated Ca_2CoO_3 layers can be detected. This suggests that neither one of these structural defects has any influence on the doping (or mobile hole concentration) in the CoO_2 layers.

Figures 2(e) and 2(f) show the O *K*-edge taken from the CoO_2 and the Ca_2CoO_3 layers, as well as the CoO_2 stacking faults. The O *K*-edge for all positions shows a strong prepeak centered at 533 eV and split into two distinct peaks, which stem from transitions into the hybridized Co 3*d* t_{2g} and e_g orbitals. This feature is followed by a shoulder located about 10 eV above the edge onset, which is due to transitions from the O 2*p* to the Ca 4*s* orbitals.

As can be seen in Figs. 2(e) and 2(f) the O *K*-edge prepeak has the lowest intensity in the CoO columns in middle of the Ca_2CoO_3-layer, but shows the strongest intensity in the shoulder 10 eV above the edge onset. This can be explained by the lower Co valence and the stronger bonding between CaO and CoO in the Ca_2CoO_3-layer. The O *K*-edge prepeak in the CoO_2 layer shows a distinct increase due to the higher Co valence

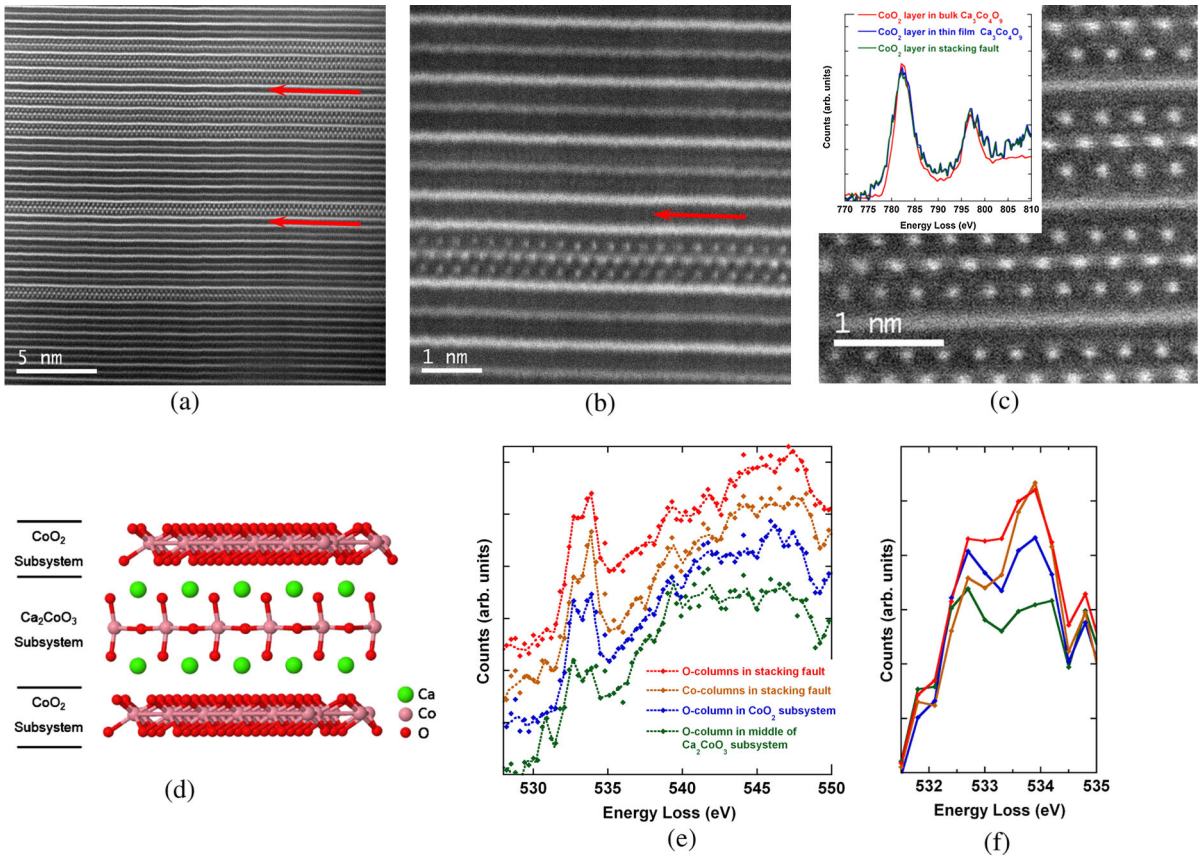

FIG. 2 (color online). Z-contrast image of $Ca_3Co_4O_9$-thin film along the [110], (a) low-magnification image showing several stacking faults (indicated by arrow) and $Ca_3Co_4O_9$ layers with interlayer rotation, (b) enlarged view of (a). (c) Bulk $Ca_3Co_4O_9$ [110] without any stacking faults or interlayer rotation. Insert: Comparison of the Co *L*-edge taken from bulk $Ca_3Co_4O_9$ and the thin film. (d) ball-and-stick model of $Ca_3Co_4O_9$ [110]. (e) EEL spectra from the different layers. Spectra are offset vertically to emphasize the changes in fine structure. (f) Enlarged prepeak intensity without vertical offset.

and the presence of mobile holes in the CoO_2x layers [18,20]. The intensity of the two prepeaks is still very similar, but the second peak appears to have shifted approximately 0.4 eV towards lower energy compared to the Ca_2CoO_3-layer. The O K-edge spectra obtained from the CoO_2 stacking faults show a further increase in the prepeak intensity.

The spectra taken from the Co and O atomic columns within the stacking fault show an increase in the peak located at 533.9 eV, while the intensity ratio between the two prepeaks is significantly different for each position. The intensity ratio between the first and second prepeak in the CoO_2 layers is 0.95, this ratio drops to 0.72 and 0.85 for the Co and O atomic columns in the stacking fault, respectively. We notice that the Co L-edge and O K-edge taken from CoO_2-layers at the boundary between two rotated $Ca_3Co_4O_9$ layers does not show any significant difference compared to $Ca_3Co_4O_9$ bulk (Supplemental Materials Fig. S3 [17]).

To further understand the reason for the higher prepeak intensity in the CoO_2 stacking faults and its influence on the thermoelectric transport properties, we study the possible mechanisms that give rise to the observed changes in the O K-edge prepeak intensity. It was previously reported that the O K-edge prepeak intensity is a sensitive measure of the Co^{3+} spin state in cubic perovskite system [21], and the splitting of the O K-edge prepeak stems from the Ligand-field splitting of hybridized Co $3d$ orbitals into t_{2g} and e_g. Since the spectra for Co^{3+} do not exhibit any splitting of the O K-edge prepeak [22], the changes in the O K-edge prepeak intensity could either indicate either an increased Co valence state or a higher spin state of the Co^{4+} ions in the CoO_2 stacking faults.

As we have shown earlier, the Co valence state remains unchanged in the CoO_2 stacking faults, and an increased concentration of Co^{4+} ions would also result in an overall decrease in the Seebeck coefficient [see Fig. 1(b)]. We therefore propose that the increase in the O K-edge prepeak intensity stems from a different occupancy of the Co^{4+} t_{2g} and e_g orbitals, as the result of an increased spin state of the Co^{4+}-ions. Such a spin-state transition can explain the observed increase in the in-plane Seebeck coefficient, since the combination of Co^{3+}-ions in the low spin state and Co^{4+}-ions in the intermediate spin state will result in a significantly higher Seebeck coefficient. It was previously suggested that such a spin-state transition occurs at 420 K in bulk $Ca_3Co_4O_9$ and is responsible for the observed changes in electrical resistivity and the increasing Seebeck coefficient above 420 K [20,23]. Earlier calculations by Landron *et al.* [24] have shown that the orbital degeneracy of the Co^{4+} ions in CoO_2 strongly depends on the Co-O bond-angle, which is directly correlated to the energy of the a_{1g} and e_g' orbitals. Therefore, an alternative explanation for the measured increase in the Seebeck coefficient could be that the introduction of extra layers in the stacking fault will distort the CoO_2 octahedra and thereby impact the filling and the relative positions of these orbitals. Consequently, the spin degeneracy of the Co^{4+} ions is increased, resulting in an increasing Seebeck coefficient. Such a model does not, however, explain the observed increase in the O K-edge prepeak intensity, since changing the occupancy of the a_{1g} and e_g' orbitals should only change the shape, but not the overall intensity of the O K-edge prepeak.

To further explore the observed changes in the near-edge fine-structure of the O K-edge, first-principles density functional theory (DFT) calculations were performed on an approximated unit-cell for $Ca_3Co_4O_9$. The incommensurate structure was modeled with a 66 atom cell [25]. The electronic structure was then calculated using the projector-augmented wave method and the generalized gradient approximation.

The calculated fine-structure of the CoO layers [Fig. 3(a)] reproduces the experimentally observed prepeak splitting. Furthermore, by comparing the experimental prepeak intensity ratio with the calculated spectra, we find that the O K-edge prepeak in the CoO layer mostly represents the in-plane Co-O bonding (i.e., p_x and p_y), with a measured energy difference between the peaks, $\Delta d = 1.3$ eV, close to the calculated value of 0.9 eV. For the CoO_2 layer, the splitting is again reproduced by the calculations, but the modeled Δd is smaller than in the CoO layer. The predicted shift of the prepeak intensity in the CoO_2 layers was not, however, observed experimentally, which is attributed to the limitations of using a small, approximate unit cell in our calculations.

As expected, the out-of-plane (i.e., p_z) Co-O bonding is significantly enhanced in the CoO_2 layers, represented by the high intensity peak located at 532.6 eV in the

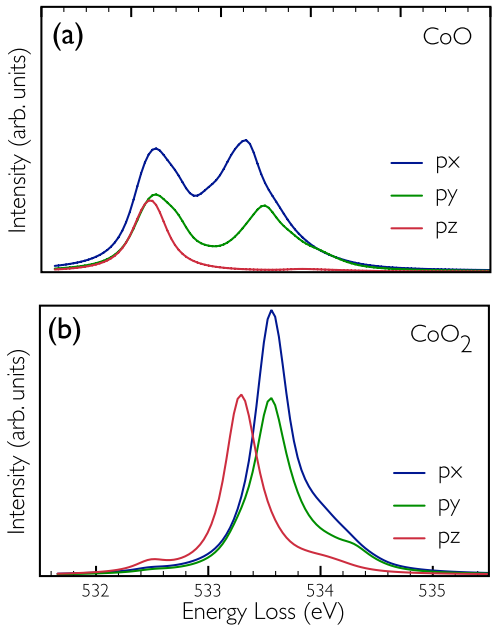

FIG. 3 (color online). Calculated O K-edge spectra for (a) the Ca_2CoO_3 and (b) the CoO_2 layers.

experimental spectra, while the peak at 533.9 eV is attributed to the in-plane (p_x, p_y) Co-O bonding. The observed changes in the prepeak intensity ratio within the CoO_2 stacking faults, in particular, the increased intensity of the second prepeak, appear to stem from additional contributions of the p_x and p_y states. The higher intensity of the first prepeak in the O columns compared to the Co columns in the stacking fault is attributed to a higher concentration of p_z states. This increase in the density of p_z states could be attributed to an increased strain in the stacking fault or a difference in the interlayer bonding due to the presence of two CoO_2 layers. We have previously shown that the first O K-edge prepeak in the experimental data [Fig. 2(f)] stems from transitions into the Co t_{2g} orbitals which correspond to the lowest energy empty states above E_f shown in our DFT calculations, i.e., the p_z states [Fig. 3(b)]. We can, therefore, directly relate the measured changes in the O K-edge prepeak intensities to the increased density of empty Co^{4+} t_{2g} states as the result of a Co^{4+} spin-state transition.

In summary, we have shown that thin $Ca_3Co_4O_9$ films grown on $SrTiO_3$ exhibit a significant increase in the Seebeck coefficient, while the electrical resistivity remains at bulk levels. We attribute the higher Seebeck coefficient to CoO_2 stacking faults present throughout the film, which stabilize the Co^{4+}-ions in an intermediate spin state, as opposed to the low spin state found in bulk $Ca_3Co_4O_9$ at room temperature. While stacking faults generally decrease the electrical conductivity, in $Ca_3Co_4O_9$ the presence of CoO_2 stacking faults does not decrease the electrical in-plane conductivity. We attribute this to the fact that the CoO_2 layers exhibit in-plane p-type conductivity. An increased concentration will not result in a decreased in-plane conductivity. We suggest that future defect or strain engineering, in particular, the stabilization of additional CoO_2 stacking faults will result in an even higher Seebeck coefficient at room and elevated temperatures, with an upper limit of $S_{\max} \approx 280\ \mu V/K$. In addition, we expect that the stacking faults will also contribute to reducing the overall thermal conductivity. Such an improvement in the Seebeck coefficient, while maintaining a low electrical resistivity and thermal conductivity, will allow for a significant increase in zT at temperatures up to 1000 K, thereby making $Ca_3Co_4O_9$ the ideal material for many high temperature waste heat-recovery applications.

This work was supported by the NSF [DMR-0846748 (R. F. K.), DMR-0938330 (J. C. I.)], by ORNL's Shared Research Equipment (SHaRE) User Program, sponsored by the DOE Office of Basic Energy Sciences (J. C. I.), DOE [DE-FG02-09ER46554 (M. P. P., S. T. P.)], by DOE [DE-AC02-06CH11357 (S. K., B. D.)], by the McMinn Endowment (S. T. P.) at Vanderbilt University, and the U.S. Army Research Office (W911NF-10-1-0147). S. Ö. acknowledges support by the National Science Foundation under the Independent Research/Development program while working at the Foundation.

[1] M. S. Dresselhaus, G. Chen, M. Y. Tang, R. G. Yang, H. Lee, D. Z. Wang, Z. F. Ren, J. P. Fleurial, and P. Gogna, Adv. Mater. **19**, 1043 (2007).
[2] G. J. Snyder and E. S. Toberer, Nature Mater. **7**, 105 (2008).
[3] F. Gascoin, S. Ottensmann, D. Stark, S. M. Haile, and G. J. Snyder, Adv. Funct. Mater. **15**, 1860 (2005).
[4] S. Bobev and S. C. Sevov, J. Solid State Chem. **153**, 92 (2000).
[5] R. Venkatasubramanian, E. Siivola, T. Colpitts, and B. O'Quinn, Nature (London) **413**, 597 (2001).
[6] I. Terasaki, Y. Sasago, and K. Uchinokura, Phys. Rev. B **56**, R12685 (1997).
[7] Y. Y. Wang, N. S. Rogado, R. J. Cava, and N. P. Ong, Nature (London) **423**, 425 (2003).
[8] I. Matsubara, R. Funahashi, M. Shikano, K. Sasaki, and H. Enomoto, Appl. Phys. Lett. **80**, 4729 (2002).
[9] G. J. Xu, Appl. Phys. Lett. **80**, 3760 (2002).
[10] Y. F. Hu, W. D. Si, E. Sutter, and Q. Li, Appl. Phys. Lett. **86**, 082103 (2005).
[11] B. C. Zhao, Y. P. Sun, W. J. Lu, X. B. Zhu, and W. H. Song, Phys. Rev. B **74**, 144417 (2006).
[12] L. Xu, F. Li, and Y. Wang, J. Alloys Compd. **501**, 115 (2010).
[13] Q. Qiao, A. Gulec, T. Paulauskas, S. Kolesnik, B. Dabrowski, M. Ozdemir, C. Boyraz, D. Mazumdar, A. Gupta, and R. F. Klie, J. Phys. Condens. Matter **23**, 305005 (2011).
[14] Y. F. Hu, E. Sutter, W. D. Si, and Q. Li, Appl. Phys. Lett. **87**, 171912 (2005).
[15] G. D. Tang, H. H. Guo, T. Yang, D. W. Zhang, X. N. Xu, L. Y. Wang, Z. H. Wang, H. H. Wen, Z. D. Zhang, and Y. W. Du, Appl. Phys. Lett. **98**, 202109 (2011).
[16] P. Limelette, S. Hebert, V. Hardy, R. Fresard, C. Simon, and A. Maignan, Phys. Rev. Lett. **97**, 046601 (2006).
[17] See Supplemental Material at http://link.aps.org/supplemental/10.1103/PhysRevLett.108.196601 for details about the experimental and theoretical methods, transport measurements, and electron energy-loss analysis.
[18] G. Yang, R. F. Klie, and Q. Ramasse, Phys. Rev. B **78**, 153109 (2008).
[19] M. Pollet, J. P. Doumerc, E. Guilmeau, D. Grebille, J. F. Fagnard, and R. Cloots, J. Appl. Phys. **101**, 083708 (2007).
[20] G. Yang, Q. Ramasse, and R. F. Klie, Appl. Phys. Lett. **94**, 093112 (2009).
[21] R. F. Klie, J. C. Zheng, Y. Zhu, M. Varela, J. Wu, and C. Leighton, Phys. Rev. Lett. **99**, 047203 (2007).
[22] R. F. Klie, J. P. Buban, M. Varela, A. Franceschetti, C. Jooss, Y. Zhu, N. D. Browning, S. T. Pantelides, and S. J. Pennycook, Nature (London) **435**, 475 (2005).
[23] A. C. Masset, C. Michel, A. Maignan, M. Hervieu, O. Toulemonde, F. Studer, B. Raveau, and J. Hejtmanek, Phys. Rev. B **62**, 166 (2000).
[24] S. Landron and M.-B. Lepetit, Phys. Rev. B **77**, 125106 (2008).
[25] R. Asahi, J. Sugiyama, and T. Tani, Phys. Rev. B **66**, 155103 (2002).